

David B. Davidson
Dept. E&E Engineering
University of Stellenbosch
Stellenbosch 7600, South Africa
Tel: +27 21 808 4458
Fax: +27 21 808 4981
E-mail: davidson@sun.ac.za

Foreword by the Editor

Microwave detection of breast cancer is a potentially promising technology for addressing one of the scourges of modern life. This paper describes *MATLAB* tools for creating contrast maps from MRI data. These maps are required to test the inversion algorithms via a numerically rigorous forward-scattering analysis.

The editor and his family recently lost a close friend (a young mother) to breast cancer. This submission had a particular resonance with the editor, who thanks the authors for their timely contribution. The editor hopes that the work in progress in this field will ultimately assist others in the early detection of breast cancer.

Modeling Realistic Contrast Maps from MRI Images for Microwave Breast Cancer Detection

G. Angiulli, T. Isernia, and S. Tringali

DIMET, Faculty of Engineering
University Mediterranea
via Graziella 1, 89122 Reggio Calabria (RC), Italy
Tel: +39 0965/875275; E-mail: giovanni.angiulli@unirc.it; tommaso.isernia@unirc.it; salvo.tringali@gmail.com

Abstract

We describe the implementation of a **MATLAB* experimental framework for the data conversion of magnetic-resonance (MRI) images to contrast maps. This is done for use in microwave breast cancer detection via the contrast source (CS) model (although the underlying logic can be adapted quite easily to different contexts and applications). The framework is conceived to relieve interested developers from most of the programming burden, and to provide final users with a friendly, consistent approach to the numerical simulations.

Keywords: Biomedical computing; biomedical image processing; biomedical magnetic resonance imaging; cancer; microwave imaging; tumors

1. Introduction

Breast cancer is one of the most common forms of tumors among women. Regular breast examination and imaging such as X-ray mammography are suggested to promote early breast-cancer detection as an important part of effective treatment. However, the methods available so far present acknowledged limitations, such as difficulty in imaging women with dense breasts. Moreover, X-ray radiography may hardly be called noninvasive, due to destructive effects on the tissues caused by ionizing radiation. Today's X-ray techniques, although much more safe and sophisticated than before, still employ the same kind of radiation and constitute the same kind of health risks as years ago [1].

The previous considerations have generated an increasing interest in the development of new approaches. Alternative methods are often based on different physical properties of the biological tissues compared to X-ray mammography. For example, several techniques have been proposed to image electrical properties, such as the equivalent dielectric permittivity or some related quantity. Among other methods, microwave imaging is especially worthy, due to the contrast in the dielectric properties of normal and malignant breast tissues (see [2] and references therein).

To this end, many different approaches are available in the literature. Among the most popular and promising approaches, we recall conjugate-gradient methods (e.g., [3, 4]), the distorted-Born iterative method (DBIM) and equivalent Gauss-Newton methods (e.g., [5-7]), and contrast-source (CS) inversion methods (e.g., [8-10]). To obtain the best results, the corresponding procedures have to be carefully tested: this is mainly aimed at calibrating the many parameters on which their performance may be dependent. Such a preliminary analysis often exploits synthetic data, obtained from the solution of a related forward-scattering problem. It hence requires some electromagnetic model of the female breast, making apparent the demand for realistic three-dimensional numerical models of the female breast [11]. High accuracy is desired to establish whether or not the relevant algorithms are worthy and efficient. This is much more significant if one considers that so many contributions in the specialized literature on the topic use simplified models of the female breast to carry out the same investigations (e.g., two-dimensional models where a normal breast is represented as a dielectric cylinder, and all tissues except skin are homogenized). It may then be helpful to wield flexible software that compounds comfortable simulation environments and powerful data-analysis tools, so preventing the final user from the need to edit the source code in order to, say, tune the pertinent parameters. Nevertheless, building a custom program, especially if a fine user interface (UI) is desired, is a demanding task, even if high-level programming languages are employed.

In particular, the present work is focused on a common way of obtaining anthropomorphic female-breast phantoms from magnetic resonance (MRI) images. For example, these may be used to evaluate the sensitivity of the algorithms for application to microwave breast-cancer detection via contrast-source integral equations, as well as in manifold similar contexts, just taking minor changes into account. Moreover, the paper provides basic elements that may be helpful to professional practitioners and researchers in the design and development of their own experimental framework. In fact, the appropriate programs have been implemented in *MATLAB* [12].

The article is organized as follows. Section 2 reviews the mathematical setting in which the scattering problem underlying the specific application of microwave imaging has to be settled. Section 3 then describes how to obtain female-breast phantoms

from MRI images. Finally, Section 4 discusses some critical features of the applicable procedures, and a way of coding them in *MATLAB*. Conclusions follow.

2. The Contrast-Source Model

As stated in the previous section, the forward-scattering model that we take over to apply microwave imaging to breast-cancer detection resides in the contrast-source integral equations (CSIEs). With reference to the terminology and the notations introduced in the previous section, these are indeed two coupled integral equations [13], i.e.,

$$\forall \mathbf{r} \in \mathcal{D}: \mathbf{J}(\mathbf{r}) - \chi(\mathbf{r}) \mathbf{E}^i(\mathbf{r}) = \chi(\mathbf{r}) \int_{\mathcal{D}} \mathbf{G}(\mathbf{r}-\mathbf{s}) \mathbf{J}(\mathbf{s}) d\mathbf{s}, \quad (1)$$

$$\forall \mathbf{r} \in \Gamma: \mathbf{E}^s(\mathbf{r}) = \chi(\mathbf{r}) \int_{\mathcal{D}} \mathbf{G}(\mathbf{r}-\mathbf{s}) \mathbf{J}(\mathbf{s}) d\mathbf{s}, \quad (2)$$

where $\mathbf{G}(\bullet)$ stands for the dyadic Green function associated with an unbounded $\tilde{\epsilon}_b$ -homogenous space; $\mathbf{E}^i(\bullet)$ is the *incident field*, i.e., the field that would exist in any point of the space once the breast has been removed; $\mathbf{E}^s(\bullet)$ is the *scattered field*, i.e., the field resulting from the interaction between the incident field and the biological tissues; $\mathbf{J}(\bullet)$ is the equivalent current density through the domain \mathcal{D} , geometrically corresponding to the hole where the patient's breast is immersed; and Γ denotes any three-dimensional curve on which the scattered field must be evaluated. The quantity

$$\chi(\bullet) = \frac{\tilde{\epsilon}(\bullet)}{\tilde{\epsilon}_b} - 1$$

is the *contrast function*: it expresses the relationship between the complex equivalent permittivity of the electromagnetic scenario and the equivalent permittivity of the surrounding medium.

Here, we have in mind a confocal microwave-imaging system in which the patient lies prone with her breast extending through a cylindrical hole in the examining table. The (theoretically unbounded) region \mathcal{D}_b around the breast is completely filled with some (ideally homogenous) matching liquid. This is referred to as the *background* or the *host medium*, and it presents a constant equivalent permittivity, $\tilde{\epsilon}_b$, whereas the tissues have an equivalent permittivity, $\tilde{\epsilon}(\bullet)$, varying from point to point. As a consequence, $\chi(\mathbf{r}) = 0$ for any $\mathbf{r} \in \mathcal{D}_b$. The integral operators $\mathcal{A}_i[\bullet]$ and $\mathcal{A}_e[\bullet]$, which are implicitly defined by Equations (1) and (2), describe the way in which the scattered field is related to the equivalent current, $\mathbf{J}(\bullet)$, on the points of \mathcal{D} and Γ , respectively.

In simple words, microwave cancer detection via the contrast-source integral-equation model is based on the expectation that the presence and positions of any possible biological lesions can be diagnosed via the contrast imaging of the breast tissue. In preliminary research, anyway, the approach is reversed. A certain contrast map is assumed to represent a *normal* reference scenario Ω (e.g., a sane breast). This is subsequently altered by the artificial insertion of one or more fake tumors. The result is a slightly different scenario, $\Omega + \delta\Omega$. Both Ω and $\Omega + \delta\Omega$ are subsequently illuminated with the same incident field, \mathbf{E}^i , and the resulting scat-

tered fields, \mathbf{E}^s and $\mathbf{E}^s + \delta\mathbf{E}^s$ are computed via appropriate procedures solving two related forward-scattering problems. The *residual field*, $\delta\mathbf{E}^s$, can then be used to measure the discrepancy of $\Omega + \delta\Omega$ from the reference scenario Ω , for example in order to gain increased understanding of the problem (e.g., understanding relationships between input and output variables) or to enhance model development (e.g., refining the model itself).

3. From MRI Images to Contrast Maps

From the perspective of mathematical modeling, Ω and $\Omega + \delta\Omega$ represent subsets of the Cartesian product $\mathbb{R}^3 \times \mathbb{C}^p$. More precisely, they are the graphs of certain functions $\mathcal{D} \subseteq \mathbb{R}^3 \rightarrow \mathbb{C}^p$, where \mathcal{D} is the (geometric) three-dimensional support of the hole in which the patient's breast is immersed during the screening, and p is the number of (complex) scalar parameters associated with every single point of \mathcal{D} that are relevant with respect to the specific diagnostic application. In particular, when dealing with the contrast-source integral-equation model, there exists a unique parameter involved in the analysis, i.e., the contrast function $\chi(\cdot)$, so $p=1$.

Actually, up to some suitable affine transformation, the geometric domain \mathcal{D} can be discretized to a finite Cartesian grid \mathcal{R} of the integer lattice \mathbb{Z}^3 with a finite resolution $s_x \times s_y \times s_z$. Each of its cells C_i is characterized by an array (x_i, y_i, z_i) of half-integer coordinates, corresponding to the centroid of the volume element $V_i \subseteq \mathcal{D}$ associated with C_i ; and a p -uple $(\xi_1, \xi_2, \dots, \xi_p) \in \mathbb{C}^p$, representing the mean values of the relevant electromagnetic parameters in V_i .

Adjoining the geometric data relative to the lattice coordinates of an arbitrary cell of \mathcal{R} to the corresponding p -uple $(\xi_1, \xi_2, \dots, \xi_p)$ defines a voxel. A voxel represents the sub-volume box with a constant scalar/vector value inside, which is equal to the scalar/vector value of the corresponding grid of the original discrete representation of the volumetric data. Voxel data sets have a limited resolution, as precise data is only available at the center of each cell. This is analogous to a pixel, which represents two-dimensional image data in a bitmap. Voxels are frequently used in the visualization and analysis of medical and scientific data. Indeed, a notable example is provided by magnetic-resonance imaging (MRI), especially in case where realistic numerical phantoms (of glands, organs, or portions of entire apparatuses) are required as test beds for preliminary investigations.

In the following, to be concrete and to explain the usage of MRI images for applications to breast-cancer detection via the contrast-source integral-equation model, we take for reference the numerical phantoms that UWCEM (University of Wisconsin-Madison Computational Electromagnetics Laboratory) makes available online for free at the URL given in [14]. Apart from a plain text file (`BreastInfo.txt`) giving some useful details about the imaged breast (such as the resolutions $s_x \times s_y \times s_z$ of the three-dimensional grid \mathcal{R} in units of grid cells, with respect to the coordinate axes in the system shown in Figure 1), the UWCEM phantoms are composed of two ASCII files, namely `mtype.txt` and `pvalue.txt`. Both consist of a single column of data, with each row representing a different voxel in the uniform Cartesian

grid \mathcal{R} of the MRI image. Moreover, UWCEM dispatches any further information about the pattern used to write down the data on file.

The i th row of the `mtype.txt` file contains one of a finite number of media numerical identifiers (IDs). Each ID corresponds to a particular tissue: the immersion medium ID is assigned to all voxels outside of the breast, the muscle medium ID is used to mark any voxel in the chest-wall region, and media IDs associated with normal breast tissues are attached to all voxels within the breast interior and the subcutaneous fat layer at the base of the breast. In particular, the UWCEM MRI images categorize the normal breast tissues into seven types, ranging from the highest-water-content fibroconnective/glandular tissue with the highest dielectric properties, to the lowest-water-content fatty tissue with the lowest dielectric properties.

In a similar fashion, the i th row of the `pval.txt` file provides information about the conductivity and the dielectric properties of the imaged breast. The format is also single column, and the file was generated using the same voxel ordering as `mtype.txt`. In `pval.txt`, each voxel that represents normal breast tissue or subcutaneous fat has an associated value ρ within the range $[0;1]$, where lower values correspond to lower dielectric properties values of ρ within the given tissue type, and higher values correspond to higher dielectric properties values. The values of ρ for all other voxels are set to zero.

Once the user has fixed some operating frequency, the data coming from `mtype.txt` and `pval.txt` can be combined to obtain maps for the equivalent dielectric permittivity of the breast tissues according to any variant of the standard procedure outlined in [15]. This requires some dispersion model. Popular choices are the one-pole Debye and the one-pole Cole-Cole equations [16]. Once the permittivity of each voxel has been calculated starting from the MRI data, the three-dimensional contrast function $\chi(\cdot)$ can be finally derived, and the processing may go on to the next steps.

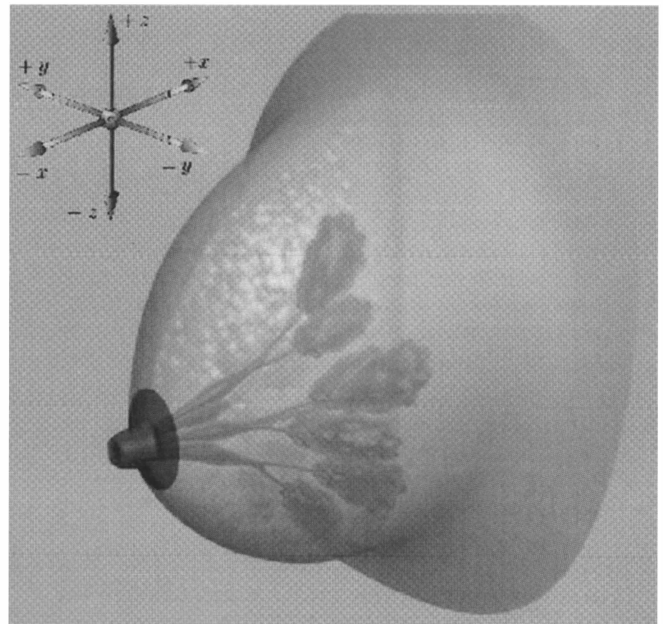


Figure 1. A three-dimensional view of a female breast, showing the coordinate system employed in the paper.

4. A worked-Out Solution

Our sample program to convert MRI images to three-dimensional contrast maps is coded in *MATLAB*. It is essentially based on a terminal user interface (TUI). It can process one MRI image per time, even if it may produce more output contrast maps per simulation (while iterating through the operating frequencies and the equivalent permittivity of the host medium). The purpose is also to provide guidelines for anyone interested to the design and development of their own program for experimental research in the field of microwave breast-cancer diagnostics via the contrast-source integral equation or related mathematical models.

4.1 Parameters and Combinations Thereof

Three structures (say, `breast`, `setup`, and `tumors`) are employed for setting the appropriate simulation parameters, and to let the user make different choices for different applications. Structures are special *MATLAB* arrays: they resemble *C++* classes, allowing for a reasonable tradeoff between flexibility and ease [17]. The structure `breast` contains general information about any given MRI image to be processed, and, subsequently, about the right way in which it must be processed. In particular, the structure has the following dummy fields:

- `path`: the path to the local or remote directory containing all the parts of any given MRI image needed for its conversion to a contrast map.
 - `model`: a string indicating which dispersion equations have to be used in order to model the dependence of the relevant electromagnetic properties (e.g., the conductivity and the dielectric permittivity) on the operating frequency.
 - `format`: a string indicating the expected format in which the input raw data are packaged, hence the right way to load them into the workspace of *MATLAB* and, then, to process them. For example, if `format` has the value 'UWCEM', then the program assumes that input MRI images consist of two files, the formats of which reflect the logic outlined in Section 3.
 - `in_resolution`: a linear 3-array of positive integers giving the full resolution $s_x \times s_y \times s_z$ of input MRI images.
 - `out_resolution`: a linear 3-array of positive integers giving the reduced resolution $r_x \times r_y \times r_z$ of the output contrast maps after being eventually resized.
 - `padding`: a string indicating if and how to pad a given input MRI image by adding around it some extra voxels in order to make a perfect cube whenever the original resolution $s_x \times s_y \times s_z$ does not fulfill the condition $s_x = s_y = s_z$. This may be necessary to insure that the cells of the output resized contrast maps still have uniform length along the three coordinate axes.
 - `voxel_edge`: a positive real expressing the length (in meters) of the edge of any cell of the three-dimensional uniform Cartesian grid of which MRI images consist.
 - `resize`: a string indicating which kind of resize must be applied to the contrast maps obtained from full-resolution MRI images.
- In a similar way, `setup` serves to assign specific values to the parameters of the diagnostic system. In particular, the fields of `setup` are as follows:
- `background`: a structure that indicates the electromagnetic properties of the immersion medium. This is accomplished by means of two linear arrays of real numbers of the same length (say, `eps` and `sigma`), where the user specifies the relative permittivity and the conductivity (in S/m) to be processed in the course of one single simulation.
 - `frequency`: a linear array of positive real numbers corresponding to the operating frequencies that must be iteratively analyzed in the course of a single simulation.
- Finally, the third structure (`tumors`) is used to define the number n_t , the position and the electromagnetic characteristics of the tumoral masses artificially implanted inside the breast, assuming these all are spherical. In particular, `tumors` includes the following fields:
- `number`: a positive integer expressing the number, n_t , of fake tumors to be inserted.
 - `position`: this is either a string or an array of n_t rows and three columns containing the coordinates (in grid units) of the centers of the fictitious tumors that the user places in the breast tissues. As a string, `position` may assume uniquely the value 'manual'. In this case, the program opens a graphical user interface (GUI), and serially shows n_t random slices of the breast's three-dimensional contrast image, so allowing the user to position the fake tumors by a simple point & click procedure.
 - `radius`: a linear array of positive integers giving the radius (in grid units) of the sphere modeling the i th fake tumor, for $i = 1, 2, \dots, n_t$. Depending on `tumors.position`, the program checks to see if the tumors are sufficiently small that they do not extend outside the inner sub-region of the domain \mathcal{D} bounded by the skin.
 - `EM_info`: an array of n_t by two positive real numbers giving the relative permittivity and the conductivity (in S/m) of the i th fake tumor, for $i = 1, 2, \dots, n_t$.

4.2 Outline of the Logical Flow of the Programming

Let us consider the logical flow outlined by the block diagram in Figure 2 and the reference variables defined in the upcoming section. First, the user sets the relevant simulation parameters assigning appropriate values to the fields of the structures `breast`, `setup`, and `tumors`.

After the program has performed all the necessary functions to check that these are presented in the expected format, all the

parts of the input MRI image are loaded into the *MATLAB* workspace. In particular, if `breast.path` has char value ‘manual’, then the user is allowed to browse through the directories of the operating system (OS), and select the local or remote repository that contains the input raw data (see Figure 3). The program then iterates through the operating frequency and the equivalent permittivity of the host medium, according to the values in the fields `frequency` and `background` of the structure setup. In particular, provided that the variables `f` and `epsb` store the operating frequency and the (complex) equivalent permittivity of the immersion liquid at an arbitrary step of the resulting double loop, then the program calculates the equivalent permittivity of all the breast tissues distinguished by the specific input MRI image on the basis of the field `breast.repository`. This requires an ad hoc implementation of the loading procedures, depending on the specific repository that the user happens to select and an a priori knowledge about the format of the MRI images retrieved from it, and uses the common switch-case paradigm. In any case, the result must be a linear array `MRI_eps` with the values of the (complex) equivalent permittivity (calculated on the basis of the dispersion model that has been specified by the field `breast.model`) of all the material media (i.e., background and biological tissues) that are distinguished in the input MRI image. The program can then compute the contrast map at the full resolution $s_x \times s_y \times s_z$, resulting from the variables `sx`, `sy`, and `sz`. Furthermore, the contrast map is possibly padded according to the rules defined by the field `breast.padding`. If required, padding introduces compensation offsets along the three coordinate directions of the underlying Cartesian grid. These are calculated by an external routine and stored in the variables `offx`, `offy`, and `offz`, provided that `chi(1, :, :)` represents the yz section of any given contrast maps that are maximally distant from the chest wall (see the orientation of the x , y , and z axes with regard to the Cartesian system in Figure 1).

Here, some care is needed in order to insure that the contrast is exactly zero at the voxels corresponding to the host medium. In presence of padding, the code homogeneously reproduces the osseous and muscle tissues at the breast base, from the side of the thorax (see Figure 4). The output is a three-dimensional array representing the point-wise value of the contrast function $\chi(\bullet)$ throughout the region of interest: this enters as a relevant function in the kernel of the linear operator $\mathcal{A}_t[\bullet]$ involved in Equation (1). It is then time for the insertion of the fake tumors to alter the normal status of the breast tissue. These are modeled as little homogeneous cubes. They are positioned according to the field position of

the input data structure `tumors`. In particular, the user has two different possibilities: either to provide the coordinates in grid units of the centers of all the fake masses to be included, or to allocate them manually by point & click through a simple graphical interface (see Figure 5) along the transversal plane at a random position generated by the program. Dimensions and electromagnetic characteristics of tumors are assigned by the fields `tumors.radius` and `tumors.ED_info`, respectively. The program (Figure 6) executes a real-time control to check that the inclusions are correctly positioned and small enough to stay confined inside the physical bounds of the skin layer.

From another viewpoint, handling full-resolution contrast maps may be quite prohibitive in terms of resources and simulation time. Hence, a mandatory step, which often precedes any subsequent processing, consists of an appropriate data resize from the full resolution, $s_x \times s_y \times s_z$ (resulting from the original MRI images and any possible padding operation), to some coarser resolution, $r_x \times r_y \times r_z$. This may be quite useful to speed up simulations and to reduce their complexity (e.g., see [19]). Our program implements such a step through different approaches that are selected just by setting the field `breast.resize` to appropriate values. Hereafter, we consider the simplest case, when `breast.resize` is assigned to a positive integer, m .

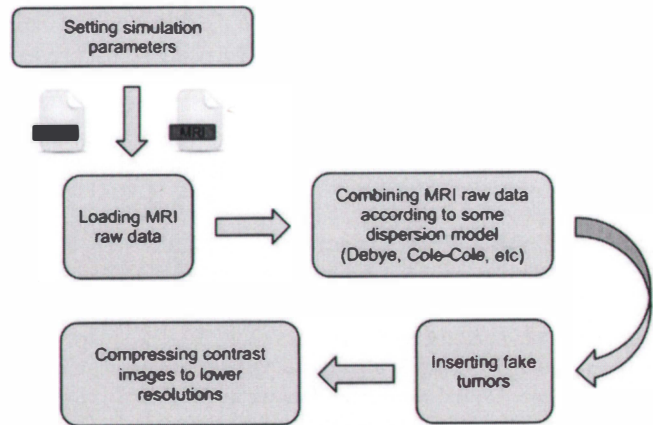


Figure 2. A block diagram showing the logical flow of the *MATLAB* code for the conversion of MRI images to contrast maps.

```

1. if ~isfield(breast, 'path') || isempty(breast.path) || ...
2.     ~ischar(breast.path) || length(size(breast.path))>2 ...
3.     || min(size(breast.path))>1 || strcmp(breast.path, ...
4.     'manual') || ~isdir(breast.path)
5.     breast.path = uigetdir(cd, ['Pick a path to a ', ...
6.     'local repository of MRI images.']);
7.     if breast.path == 0
8.         fprintf('You picked an invalid path.\n')
9.         return
10.    end
11. end
  
```

Figure 3. The code fragment that imports MRI raw data from a local or remote repository into the *MATLAB* workspace.

```

1. chi = zeros(sx+offx,sy+offy,sz+offz);
2. chi(offx+1:offx+sx,floor(offy/2)+1:floor(offy/2)+sy, ...
3.   floor(offz/2)+1:floor(offz/2)+sz) = MRI_eps/epsb - 1;
2. x_liquid = find(abs(chi(:,offy+1,offz+1))==0,1,'last');
3. for x = x_liquid+1 : 1 : offx + sx
4.   if offy > 0, chi(ii,1:offy,:) = ...
5.     chi(x,offy+1,offz+1); end
6.   if offz > 0, chi(ii,:,1:offz) = ...
7.     chi(x,offy+1,offz+1); end
8.   if offy+s2 < dy, chi(ii,offy+s2+1:dy,:) = ...
9.     chi(x,offy+1,offz+1); end
10.  if offz+s3 < dz, chi(ii,:,offz+s3+1:dz) = ...
11.    chi(x,offy+1,offz+1); end
12. end

```

Figure 4. The *MATLAB* code excerpt that if required zero pads contrast maps at their natural resolution, so that the resulting images have equal resolution along the appropriate coordinate axes, as specified by the user.

Indeed, suppose that $v_1^{(i)}, v_2^{(i)}, \dots, v_r^{(i)}$ is any enumeration of the voxels in the contiguous cluster of $r_x \times r_y \times r_z$ grid cells framed by the mobile window on its i th scanning through the (eventually) padded and full-resolution contrast map, where $r := r_x \times r_y \times r_z$ for notational convenience. The corresponding contrast, $\chi_{rd}^{(i)}$ on the reduced map is assumed equal to

$$\chi_{rd}^{(i)} = \left\{ \frac{1}{r} \sum_{k=1}^r [x_k^{(i)}]^m \right\}^{1/m}, \quad (3)$$

i.e., to the generalized mean with exponent m of the contrast values $\chi_1^{(i)}, \chi_2^{(i)}, \dots, \chi_r^{(i)}$ associated with $v_1^{(i)}, v_2^{(i)}, \dots, v_r^{(i)}$, respectively. This is implemented by an external subroutine, as described by the code fragment in Figure 7. Obviously, the shrinking technique we have just described has some limitations with respect to the minimal resolution of the output contrast maps. In fact, in order to preserve significant details of the original MRI images such as the skin, the output resolution cannot be reduced by too large a factor. Particular care must be used to prevent the skin from being smoothed too much by the process of resizing. This may imply larger than necessary computational burden and storage requirements. However, the problem is not really serious when thinking of an implementation of the appropriate procedures on modern cost-effective GPGPU computing platforms.

An ultimate fundamental aspect to account for while resizing the contrast maps is the spatial resolution of the resulting image. Some control is then necessary to check that the output resolution of the processed contrast maps fulfills Richmond's sampling rule with respect to the current operating wavelength, λ (see [13] and references therein).

In some more detail, let c_0 be the speed of light in the empty space ($c_0 = 2.9979 \times 10^8$ m/sec), and let ℓ_x, ℓ_y, ℓ_z be the lengths (in meters) of the edges of the elementary cell in the uniform grid of the resized contrast map (we can assume $\ell_x = \ell_y = \ell_z$, as far as uniform padding has been accomplished). Richmond's rule then imposes that

$$20 \max(\ell_x, \ell_y, \ell_z) \leq \min(\lambda_b, \lambda_t), \quad (4)$$

where λ_t is the minimum modulus of the wavelengths $\lambda_1, \lambda_2, \dots$ associated with the breast tissues that are discriminated by the specific MRI images the user is handling, and λ_b is the wavelength of the host medium.

5. An Application Example

We have run our code on the MRI image of a scattered fibroglandular breast from the UWCEM online phantom repository [14]. The original resolution of the image was $258 \times 253 \times 251$ grid

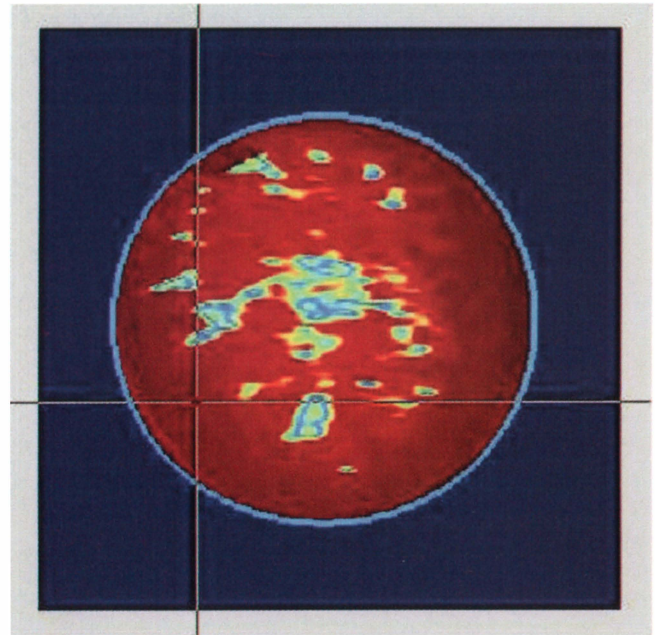


Figure 5. A screenshot of the *MATLAB* graphical user interface (GUI) for the manual positioning of fake tumors by point & click.

```

1. color_max = max(max(max(abs(chi))));
2. if ischar(tumors.position) && strcmp(tumors.position, ...
3.     'manual')
4.     tumors.position = zeros(tumors.number,3);
5.     for t = 1:1:tumors.number
6.         fg = figure('Visible','off');
7.         tx = rand(1);
8.         tx = 0.5*tx + 0.95*(1-tx);
9.         tx = floor(skin_xmax*tx+(1-tx)*skin_xmin);
10.        imagesc(abs(squeeze(chi(tx, :, :))));
11.        caxis([0,color_max])
12.        axis image, axis xy
13.        set(gca,'xtick',[],'ytick',[])
14.        ax = axis; set(fg,'Visible','on');
15.        while(1)
16.            [zt,yt] = ginput(1); yt = fix(yt); zt = fix(zt);
17.            % skin_chi is the contrast of the skin
18.            if any(chi(tx,yt-1:1*tumore.voxel,zt)==skin_chi) || ...
19.                any(chi(tx,yt,zt-1:1*tumore.voxel)==skin_chi)
20.                errordlg(['Tumors cannot be so near to the 'skin'])
21.                uiwait(); continue
22.            end
23.            tumors.position(k,:) = [tx, yt, zt];
24.        end
25.        close(fg)
26.    end
27. end

```

Figure 6. The *MATLAB* code fragment that implements the graphical user interface (GUI) for the manual positioning of fake tumors.

```

1. function B = mean_resizing(A,ind_min,ind_max,ss,rr,m)
2.
3. im = ind_min(1); jm = ind_min(2); km = ind_min(3);
4. iM = ind_max(1); jM = ind_max(2); kM = ind_max(3);
5. B = zeros(iM-im+1, jM-jm+1, kM-km+1);
6. s1 = ss(1); s2 = ss(2); s3 = ss(3);
7. r1 = rr(1); r2 = rr(2); r3 = rr(3);
8.
9. for ii = im:1:iM
10.    for jj = jm:1:jM
11.        for kk = km:1:kM
12.            i_min = 1+floor(s1*(ii-1)/r1);
13.            i_max = ceil(s1*ii/r1);
14.            j_min = 1+floor(s2*(jj-1)/r2);
15.            j_max = ceil(s2*jj/r2);
16.            k_min = 1+floor(s3*(kk-1)/r3);
17.            k_max = ceil(s3*kk/r3);
18.            B(ii-im+1, jj-jm+1, kk-km+1) = ...
19.                sum(sum(sum(A(i_min:i_max, j_min:j_max, ...
20.                    k_min:k_max).^m))^(1/m)/((k_max-k_min+1)* ...
21.                    (j_max-j_min+1)*(i_max-i_min+1)));
22.        end
23.    end
24. end

```

Figure 7. The *MATLAB* code excerpt that if required reduces contrast maps from a given input resolution to a given output resolution.

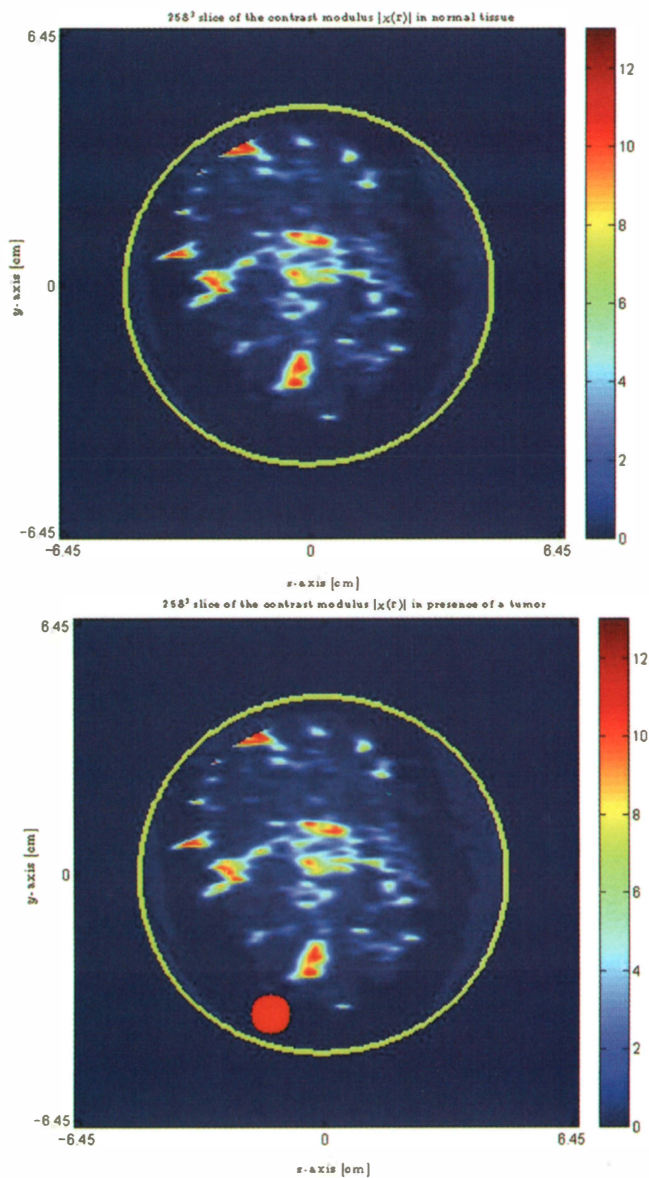


Figure 8. A transverse slice of a three-dimensional image showing the complex modulus of the breast contrast $\chi(r)$ at the full-resolution of 256^3 voxels, before (top) and after (bottom) the positioning of a fake tumor.

units. We padded it with respect to all the coordinate planes, so raising its resolution to $258 \times 258 \times 258$ grid units. The padded image was subsequently converted to a contrast map, assuming an operating frequency of 2.5 GHz and a lossless background of relative permittivity $\epsilon_b = 5$. We then inserted (by point & click) one fake tumor of 1 cm radius, after randomly assigning its transverse x coordinate via the field position of the structure tumors (see Figure 8), as outlined in the previous section. Finally, we shrank the resulting map, taking an exponent $m=1$ with regard to Equation (3) and reduced output resolutions of 128^3 , 96^3 , and 64^3 grid units (see Figure 9). On a standard workstation, the overall processing time (excepting, of course, the time needed by the user to collocate by point & click the artificial inclusions) was about 90 s for an output resolution of 64^3 grid units, about 4 min for an output resolution of 96^3 grid units, and about 17 min for an output resolution of 128^3 .

6. Conclusions

This paper has presented the implementation of a *MATLAB* terminal user interface (TUI) for the conversion of magnetic-resonance (MRI) images to contrast maps. The purpose is their use in the context of microwave breast-cancer detection via the contrast-source integral equations (CSIEs) or, more generally, in view of minor changes, in the survey of forward-scattering phenomena by heterogeneous objects. The program can be a potential aid to real projects, and in fact it has been employed successfully in an ongoing research program [18]. A free-of-charge version will be made available by electronic mail on express request to the authors.

7. Acknowledgements

The present work has been partly financed by the national project “PRIN 2007 - MANFIND (MAGnetic Nanoparticles and FIELDS for Nanotechnologies and Diagnostics),” held jointly by University “Federico II” of Naples (IT), IREA-CNR of Naples (IT), and University “Mediterranea” of Reggio Calabria (IT). Moreover, the authors are deeply grateful to Paolo Martini and Alberto Tibaldi for their critical review of the manuscript.

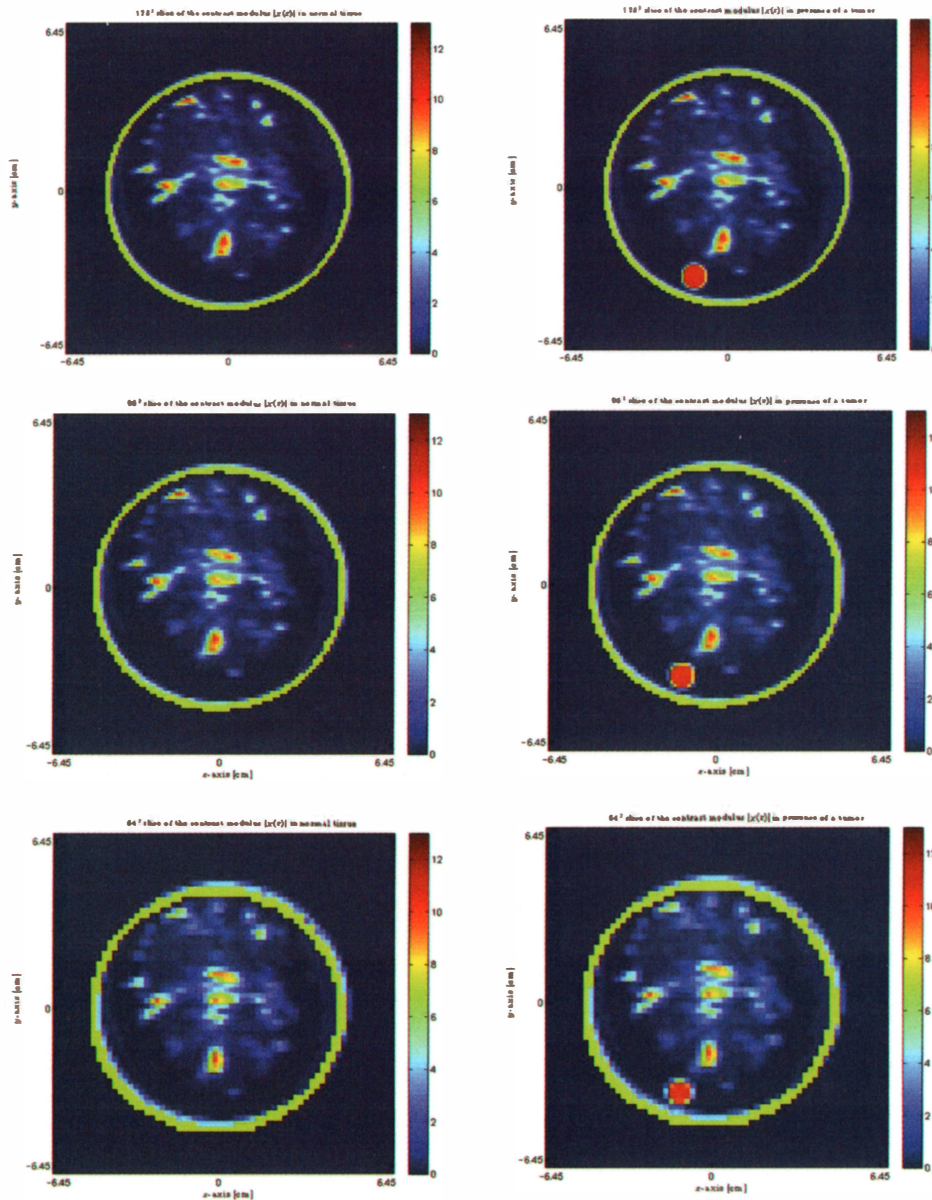


Figure 9. The same as in Figure 8, but at the reduced resolutions of 128^3 (top), 96^3 (center), and 64^3 (bottom) voxels.

8. References

1. S. K. Moore, "Better Breast Cancer Detection," *IEEE Spectrum*, **38**, 5, 2001, pp. 50-54.
2. G. A. Ybarra and Q. H. Liu, "Microwave Breast Imaging," in J. S. Suri, R. Rangayyan, and S. Laxminarayan (eds.), *Emerging Technologies in Breast Imaging and Mammography*, New York, American Scientific Publishers, 2008.
3. A. E. Bulyshev, A. E. Souvorov, S. Y. Semenov, R. H. Svenson, A. G. Nazarov, Y. E. Sizov, and G. P. Tatis, "Three-Dimensional Microwave Tomography. Theory and Computer Experiments in Scalar Approximation," *Inverse Problems*, **16**, 2000, pp. 863-875.
4. D. W. Winters, E. J. Bond, B. D. V. Veen, and S. C. Hagness, "Estimation of the Frequency-Dependent Average Dielectric Properties of Breast Tissue Using a Time-Domain Inverse Scattering Technique," *IEEE Transactions on Antennas and Propagation*, **AP-54**, 11 (2), 2006, pp. 3517-3528.
5. W. C. Chew and Y. M. Wang, "Reconstruction of 2-Dimensional Permittivity Distribution Using the Distorted Born Iterative Method," *IEEE Transactions on Medical Imaging*, **9**, 1990, pp. 218-225.
6. W. Chew, *Waves and Fields in Inhomogeneous Media*, Piscataway, NJ, IEEE Press, 1995.
7. J. D. Zaeytjij, A. Franchois, C. Eyraud, and J. M. Geffrin, "Full-Wave Three-Dimensional Microwave Imaging with a Regularized Gauss-Newton Method-Theory and Experiment," *IEEE Transactions on Antennas and Propagation*, **AP-55**, 11, November, 2007, pp. 3279-3292.

8. P. M. van den Berg and R. E. Kleinman, "A Contrast Source Inversion Method," *Inverse Problems*, **13**, 6, December, 1997, pp. 1607-1620.
9. A. Abubakar, P. M. van den Berg, and J. J. Mallorqui, "Imaging of Biological Data Using a Multiplicative Regularized Contrast Source Inversion Method," *IEEE Transactions on Microwave Theory and Techniques*, **50**, 7, 2002, pp. 1761-1771.
10. Z. Q. Zhang and Q. H. Liu, "Three-Dimensional Nonlinear Image Reconstruction for Microwave Biomedical Imaging," *IEEE Transaction on Biomedical Engineering*, **51**, 2004, pp. 544-548.
11. E. Zastrow, S. K. Davis, M. Lazebnik, F. Kelcz, B. D. Van Veen, S. C. Hagness, "Development of Anatomically Realistic Numerical Breast Phantoms with Accurate Dielectric Properties for Modeling Microwave Interactions with the Human Breast," *IEEE Transaction on Biomedical Engineering*, **55**, 12, 2008, pp. 2792-2800.
12. MATLAB, The Mathworks Inc., <http://www.mathworks.com>.
13. R. E. Kleinman and P. M. van den Berg, "Iterative Methods for Solving Integral Equations," *Radio Science*, **26**, 1, 1991, pp. 175-181.
14. The UWCEM Numerical Breast Phantom Repository, University of Wisconsin, available at <http://uwcem.ece.wisc.edu/home.htm>.
15. M. Lazebnik, L. McCartney, D. Popovic, C. B. Watkins, M. J. Lindstrom, J. Harter, S. Sewall, A. Magliocco, J. H. Booske, M. Okoniewski, and S. C. Hagness, "A Large-Scale Study of the Ultrawideband Microwave Dielectric Properties of Normal Breast Tissue Obtained from Reduction Surgeries," *Physics in Medicine and Biology*, **52**, 2007, pp. 2637-2656.
16. M. Lazebnik, M. Okoniewski, J. H. Booske and S. Hagness, "Highly Accurate Debye Models for Normal and Malignant Breast Tissue Dielectric Properties at Microwave Frequencies," *IEEE Microwave and Wireless Components Letters*, **17**, 12, 2007, pp. 822-824.
17. *MATLAB* documentation, accessible at <http://www.mathworks.com/access/helpdesk/help/techdoc/>.
18. I. Catapano, L. Crocco, L. Di Donato, G. Angiulli, T. Isernia, A. Morabito, S. Tringali, O. Bucci, "Guidelines for Effective Microwave Breast Imaging: An Accurate Numerical Assessment Against 3D Anthropomorphic Phantoms," Proceedings of the European Conference on Antennas and Propagation (EuCAP 2010), Barcelona: Spain, 2010.
19. J. D. Shea, P. Kosmas, S. C. Hagness, and B. D. Van Veen, "Contrast Enhanced Microwave Breast Imaging," 13th International Symposium on Antenna Technology and Applied Electromagnetics and the Canadian Radio Science Meeting (ANTEM/URSI 2009), Toronto, Canada, 2009. 